A HIGH SENSITIVITY HETERODYNE INTERFEROMETER AS A POSSIBLE OPTICAL READOUT FOR THE LISA GRAVITATIONAL REFERENCE SENSOR AND ITS APPLICATION TO TECHNOLOGY VERIFICATION

Martin Gohlke[1,2], Thilo Schuldt[1,3], Dennis Weise[1], Jorge Cordero[1,3], Achim Peters[2], Ulrich Johann[1], and Claus Braxmaier[1,3]

[1] *EADS-Astrium GmbH, Claude-Dornier-Straße, 88039 Friedrichshafen, Germany, E-mail: dennis.weise@astrium.eads.net*
[2] *Humboldt-Universität zu Berlin, Hausvogteiplatz 5-7, 10117 Berlin, Germany, E-mail: achim.peters@physik.hu-berlin.de*
[3] *Hochschule für Technik, Wirtschaft & Gestaltung, Brauneggerstr. 55, 78462 Konstanz, Germany, E-mail: braxm@htwg-konstanz.de*

ABSTRACT

The gravitational wave detector LISA utilizes as current baseline a high sensitivity Optical Readout (ORO) for measuring the relative position and tilt of a free flying proof mass with respect to the satellite housing. The required sensitivities in the frequency band from $30\,\mu$Hz to $1\,$Hz are $\sim$ pm/$\sqrt{\text{Hz}}$ for the translation and $\sim$ nrad/$\sqrt{\text{Hz}}$ for the tilt measurement. EADS Astrium, in collaboration with the Humboldt University Berlin and the University of Applied Sciences Konstanz, has realized a prototype ORO over the past years. The interferometer is based on a highly symmetric design where both, measurement and reference beam have a similar optical pathlength, and the same frequency and polarization. The technique of differential wavefront sensing (DWS) for tilt measurement is implemented. With our setup noise levels below 5pm/$\sqrt{\text{Hz}}$ for translation and below 10nrad/$\sqrt{\text{Hz}}$ for tilt measurements – both for frequencies above 10mHz – were demonstrated. We give an overview over the experimental setup, its current performance and the planned improvements. We also discuss the application to first verification of critical LISA aspects. As example we present measurements of the coefficient of thermal expansion (CTE) of various carbon fiber reinforced plastic (CFRP) including a "near-zero-CTE" tube.

1. INTRODUCTION

LISA – the Laser Interferometer Space Antenna – is a ESA/NASA collaborative mission, planned to be launched around 2018. Its ambition is the detection of gravitational waves in the frequency range $30\,\mu$Hz
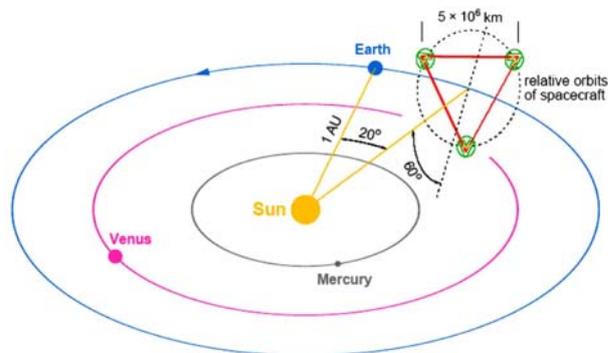
Figure 1. The three LISA spacecraft are flying in a heliocentric orbit, 20° behind the Earth. (In this schematic, the LISA triangle is enlarged by a factor of 10).

to $1\,$Hz. With a strain sensitivity of $3.2 \cdot 10^{-19}$ at a frequency of $10^{-3}\,$Hz it will detect gravitational waves caused e. g. by neutron star binaries, white dwarf binaries, super-massive black hole binaries and super-massive black hole formations.

The LISA mission consists of three identical spacecraft which form an equilateral in a heliocentric Earth-trailing orbit, approx. 20° behind the Earth (cf. Fig. 1). Each edge of this triangle – i. e. one interferometer arm – has an arm lengths of about 5 million kilometers. Gravitational waves passing the LISA formation will be measured as changes in the length of the interferometer arms by use of laser interferometry with $\sim 10\,$pm/$\sqrt{\text{Hz}}$ sensitivity.

External disturbances like solar radiation pressure or solar wind will change the position of the spacecraft and thereby might affect the interferometer signals caused by gravitational waves. Therefore, a free-flying proof mass – as part of the gravitational ref-
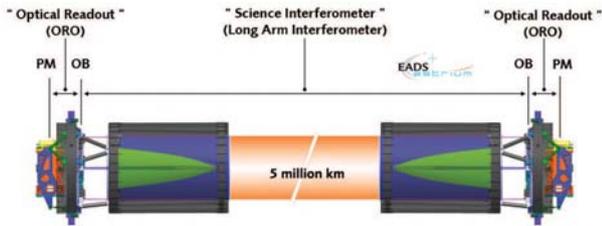
Figure 2. Schematic of the strap-down-architecture. The distance measurement is split into two local, from proof mass (PM) to the optical bench (OB), and one long distance measurement.

erence sensor (GRS) – inside the satellites is taken as reference for a purely gravitational orbit. As the external disturbances only act on the surface of the satellite, the distance between proof mass and its housing (which is rigidly connected to the satellite) is changing. In case of a drag-free controlled satellite, any change of the proof mass position is measured and the satellite is controlled in such a way that it is centered around the proof mass at any time, canceling all non-gravitational forces acting on the spacecraft. The proof mass also acts as the end mirror of the interferometer arms.

In the so-called strap-down-architecture (cf. Fig. 2 and [1]) each interferometric measurement of the distance between two satellites is split into three independent measurement: (i) the distance between the proof mass and the optical bench on the first satellite, (ii) the distance between the optical benches aboard the two satellites, and (iii) the distance between the optical bench on the second satellite and its proof mass. The proof mass position sensor is part of the so called science interferometer and must fulfill requirements of $1\,\mathrm{pm}/\sqrt{\mathrm{Hz}}$ (for frequencies above $2.8\,\mathrm{mHz}$ with an f^{-2} relaxation down to $30\,\mu\mathrm{Hz}$) for the translation measurement and at least $20\,\mathrm{nrad}/\sqrt{\mathrm{Hz}}$ for the tilt measurement (for frequencies above $0.1\,\mathrm{mHz}$ with

an f^{-1} relaxation down to $30\,\mu\mathrm{Hz}$).

These requirements necessitate an optical readout (ORO) of the proof mass position utilizing laser interferometry. Our interferometer concept is a possible ORO for the LISA sensitive axes.

2. INTERFEROMETER SETUP

Our experimental setup is based on a highly symmetric design and represents a heterodyne interferometer with spatially separated beams [2, 3, 4, 5]. Reference and measurement beams of the interferometer have the same frequency and polarization. Also, their optical pathlengths (especially inside optical components) are similar. A schematic of our interferometer setup is shown in Fig. 3, a photograph in Fig. 4.

The signal at the measurement photodiode is given by

$$I_{meas} \sim AB \cdot \cos\left(\Delta\omega t - \phi(t)\right), \qquad (1)$$

and the signal at the reference photodiode by

$$I_{ref} \sim AB \cdot \cos\left(\Delta\omega t\right). \qquad (2)$$

Here, A and B denote the amplitudes of the laser frequencies f_1 and f_2, respectively, and $\Delta\omega = 2\pi|f_1 - f_2|$. The phase $\phi(t)$ between the signals on measurement and reference photodiode is proportional to the displacement Δl of the measurement mirror:

$$\phi(t) = \frac{4\pi n}{\lambda} \cdot \Delta l(t), \qquad (3)$$

where λ is the vacuum wavelength of the light and n the refractive index of the medium the light is traveling in.

For in-quadrature measurement, the two signals

Figure 3. Schematic of the heterodyne interferometer.
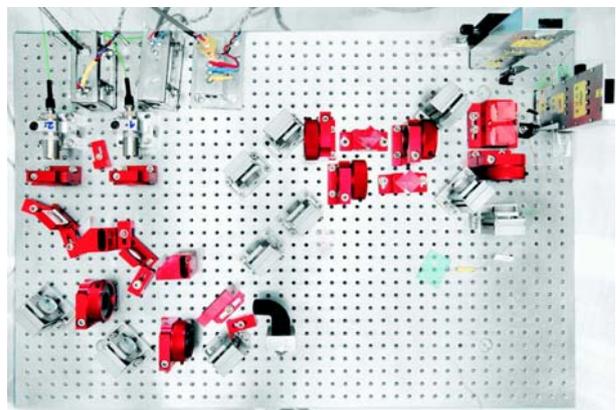
Figure 4. Picture of the interferometer board inside the vacuum chamber.

$$S_1 = \frac{1}{2} AB \cos \phi(t) \qquad (4)$$

and

$$S_2 = \frac{1}{2} AB \sin \phi(t) \qquad (5)$$

are generated, where the phase measurement is obtained by

$$\phi(t) = \tan^{-1} \frac{S_2}{S_1} . \qquad (6)$$

In order to measure the tilt of the proof mass the method of Differential Wavefront Sensing (DWS) [6, 7] is implemented. Therefore, we use quadrant photodiodes and the phase difference between opposing halves is measured. The interferometer setup can be subdivided into two parts: (i) the optical setup for frequency generation, and (ii) the interferometer board. The optics for frequency generation is placed on an optical table using standard optical components. The interferometer board is placed inside a vacuum chamber operated at pressures below 10^{-3} mbar. For mechanically stability and compactness, purpose-built optical component mounts with a beam-height of 2 cm are used.

2.1. Heterodyne Frequency Generation

An NPRO-type (non-planar ring-oscillator) Nd:YAG laser at a wavelength of 1064 nm is used as light source. Part of its output power is split and shifted in frequency by use of two acousto-optic modulators (AOMs). The AOMs are working at a frequency of 79.99 MHz and 80.00 MHz, respectively, resulting in a heterodyne frequency of 10 kHz. The two laser beams are fiber-coupled (cf. 5) and sent to the interferometer inside the vacuum chamber via optical single mode fibers. The RF-signals driving the AOMs are generated by use of two phase-locked direct digital synthesizers (DDS).

2.2. Interferometer Setup

The 300mm × 440mm × 40mm interferometer board is made by cast aluminum which offers low internal stresses and therefore reduced long-term drifts of the material. The two frequencies are fiber-coupled to the interferometer board. Polarizers at the fiber inputs and outputs ensure a proper and clean polarization. The optical power of each beam is ~ 2.5 mW at the fiber output, this is equivalent to $100 \mu W$ on the proof mass. Both beams are split at a 6 mm
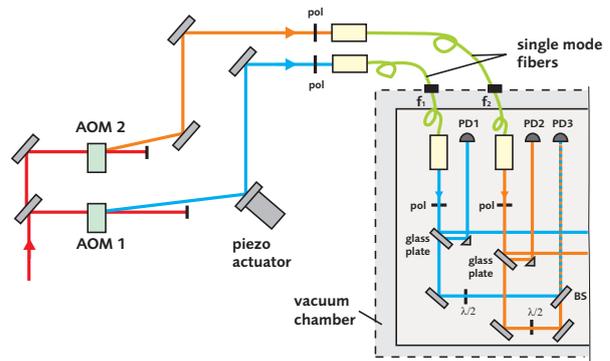
Figure 5. We use two acousto-optic modulators (AOMs) to generate the heterodyne frequency and to control the intensity of each beam (f_1 and f_2) inside the vacuum chamber. The phase lock between the beams on the interferometer board is realized by a piezo actuator outside the vacuum chamber.

thick wedged glass plate. The front side reflections are used in the interferometer while the back side reflections are sent to two monitor photodiodes (PD1 and PD2 in Fig. 3). Their signals are taken for intensity stabilization of the two laser beams after fiber outcoupling. The amplitudes of the RF signals driving the two AOMs are used for actuation of the light intensities. The beams transmitted at the glass plates are superimposed on a third photodiode (PD3 in Fig. 3). The generated heterodyne signal is phase-locked to a 10 kHz signal which is obtained by mixing the two DDS (direct digital synthesizer) output signals. The signal at the photodiode corresponds to an interferometer signal, where the splitting in measurement and reference beam takes place at the beamplitter before the AOMs outside the vacuum chamber. Therefore, it contains all differential phase effects caused by the fibers and the AOMs. A piezo-electric actuation of one mirror in one arm of the interferometer outside the vacuum chamber is used for actuation of the feedback loop. The two beams used for the interferometer are both split into two parallel output beams. A symmetric beamsplitter is used providing the same optical pathlengths inside the component. Also, ghost reflections of the input beams are not reflected back in direction of the input beam.

The beams with frequency f_1 are representing measurement and reference beams of the interferometer, the beams with frequency f_2 are used for generating heterodyne signals at the photodiodes. The beams with frequency f_1 are first reflected by a polarizing beamsplitter (PBS) towards the measurement and reference mirror, which in our experiment is realized by one fixed mirror. After passing twice a quarter waveplate ($\lambda/2$), both beams are transmitted at the PBS and superimposed with the beams with frequency f_2 at a (non-polarizing) beamsplitter (BS). Two quadrant photodiodes (QPD1 and QPD2 in Fig. 3) measure the heterodyne signals. Their sum

signals are taken for translation measurement, the signals of opposing halves for tilt measurement.

2.3. Digital Phase Measurement

The signals of the quadrant photodiode are first pre-amplified inside the vacuum chamber. The sum signals and the signals for differential wavefront sensing are generated and amplified outside the vacuum chamber by use of analog electronics. All signals are anti-aliasing filtered by use of a 6th order Bessel filter (corner frequency: 20 kHz). The signals are then simultaneously digitized by a National Instruments field programmable gate array (FPGA) computer board at a frequency of 160 kHz and with a 16 bit resolution. The FPGA board is programmed by LabVIEW. A digital phasemeter is implemented where the corresponding input signals to the FPGA board are multiplied and low-pass filtered. For in-quadrature measurement, the signals phase-shifted by 90° are generated. The data is reduced by a factor of 8000 and transferred to a LabVIEW host program which carries out the calculation as given in (6). The program also monitors phasejumps by π and therefore offers a dynamic range not limited by $\lambda/2$ in mirror translation. For the tilt measurement, the summed halves of the quadrant photodiode are input signals to the phasemeter. The obtained phase is converted to a tilt.

3. MEASURED NOISE PERFORMANCE

We performed a noise measurement where the measurement and the reference mirror are represented by the same fixed mirror (cf. Fig. 3). The power spectrum density (PSD) of the translation measurement is shown in Fig. 6, the PSD of the corresponding tilt measurement in Fig. 7. Also included in these graph are the LISA requirements. In these measurements, the intensity stabilization and the phase-lock of the heterodyne frequencies are operating. The interferometer board was not actively stabilized in temperature as it was seen, that a passive stabilization showed better results. The peak near the 3 Hz was caused by a missing synchronization of the FPGA clock and the DDS. It is removed in later measurements.

In translation measurements (cf. Fig. 6), noise level below $1\,\mathrm{nm}/\sqrt{\mathrm{Hz}}$ for frequencies above 0.1 mHz and below $5\,\mathrm{pm}/\sqrt{\mathrm{Hz}}$ for frequencies above 10 mHz were obtained. In tilt measurements (cf. Fig7) the noise level is below $1\,\mu\mathrm{rad}/\sqrt{\mathrm{Hz}}$ for frequencies above 0.1 mHz and below $10\,\mathrm{nrad}/\sqrt{\mathrm{Hz}}$ for frequencies above 10 mHz. These noise level in tilt measurement fulfil the LISA requirements for frequencies above 1 mHz.

4. APPLICATIONS

The interferometer setup as described before is a high sensitive measurement system which now can be used to investigate other key aspects in the LISA context. For example:

- determine the coefficient of thermal expansion of ultra-stable structural materials, e.g. carbon fiber reinforced plastic (CFRP),

- testing the noise performance and linearity of various LISA mechanisms, e.g. the actuator of the in-field pointing mechanism as well the mechanism itself, and

- investigate the quality of mirror surfaces in the pm-range

Figure 6. Noise measurement: Power spectrum density of the translation signal. The red curve corresponds to the LISA requirements.
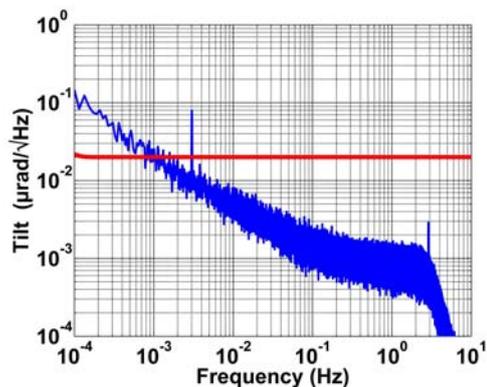
Figure 7. Noise measurement: Power spectrum density of the tilt signal. The red curve corresponds to the LISA requirements.
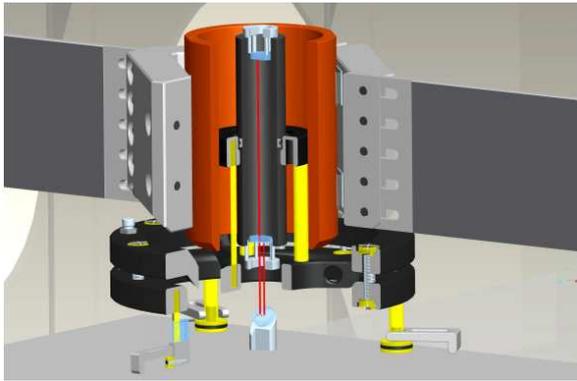
Figure 8. Cross sectioned CAD drawing of the test facility. Shown is the test tube (black, in the middle) with the mirror mounts at the top and the bottom of the tube. The test tube is surrounded by the temperature controlled copper cylinder.

4.1. Dilatometry

Based on the above presenting setup we developed a high sensitive dilatometer for characterizing the dimensional stability of ultra-stable materials. The principle of the dilatometer is shown in Fig.8. We are changing the temperature of the test tube via radiative heating/cooling and measure the linear expansion with our interferometer with sub-nm resolution. The CTE is given as:

$$CTE = \frac{1}{\Delta T} \frac{\Delta L}{L} \ [K^{-1}]. \quad (7)$$

Measurement and reference mirror are placed at the top resp. at the bottom inside a test tube made by the material under investigation (cf. Fig. 8). We also developed a test tube support, special mirror mounts and a heating/cooling system. The mirror mounts are critical components of the measurement facility, as their thermal expansion should not affect the CTE measurement of the test tube. They are made of Invar36, an iron nickel alloy with a very low CTE $(1.8 \cdot 10^{-6} K^{-1})$. The mirror is clamped inside the mirror mount, which on its part is clamped inside the test tube. The reflecting surface of the mirror and the clamping points of the mirror are all in the same plane – a thermal expansion of the mirror mount therefore should not affect the position of the reflective surface of the mirror with respect to the test tube. For measurement, a sine thermal cycling with a period up to several hours is applied to the CFRP test tube.

Due to limitations of the vacuum chamber and the interferometer setup, we are restricted to tubes with an inner diameter of 20 mm, an outer diameter of ~ 27 mm and a length of 10 cm. The temperature of the test tubes can be varied between 20° C and 60° C.

We first performed a measurement with a CFRP tube with a known CTE of $\sim -6.47 \cdot 10^{-7} K^{-1}$
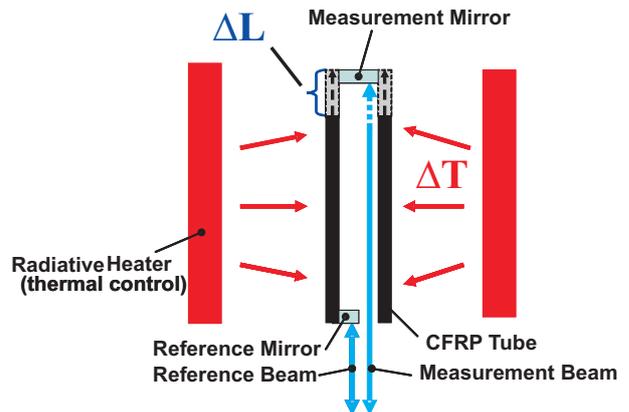
Figure 9. Sketch of the basic idea of our CTE measure facility.

(cf. Fig. 10). Our result with the interferometer test facility provided a CTE of $\sim -6.10 \cdot 10^{-7} K^{-1}$. In the next step, we procured a new CFRP tube with a theoretical CTE below $-2.5 \cdot 10^{-8} K^{-1}$. We measured a CTE of $\sim -3.6 \cdot 10^{-7} K^{-1}$, which not does not agree with the theoretical value [8].

Presently, we are and the company analyzing the manufacturing process as the determination of the CTE during production includes uncertainties.

5. SUMMARY AND OUTLOOK

We developed a compact setup of a high sensitivity heterodyne interferometer. Noise levels below $5 \, \text{pm}/\sqrt{\text{Hz}}$ in translation measurement and below $10 \, \text{nrad}/\sqrt{\text{Hz}}$ in tilt measurement – both for frequencies above 10 mHz – were demonstrated in lab experiments. In a current project, the interferometer is adapted as dilatometer for measurement of thermal expansion of carbon fiber reinforced plastics. Mea-
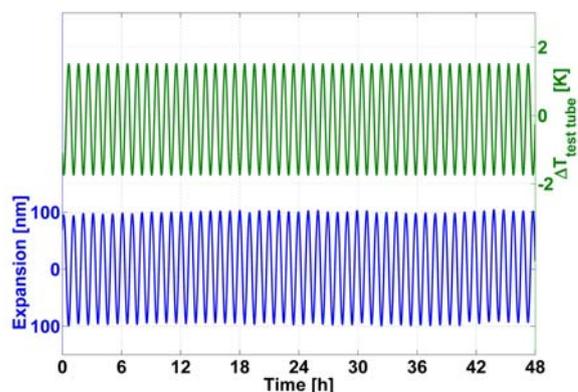
Figure 10. CTE measurement time series. The line above represents the temperature variation, the line below the expansion of the test tube.

surements were carried out validating the capability of our setup. In general, the test facility offers the possibility to characterize ultra-stable materials with a CTE down to $10^{-8}\,\mathrm{K}^{-1}$.

Current activities also include the development of new quasi-monolithic setup using thermally highly stable glass ceramics as breadboard materials in the interferometer.

6. ACKNOWLEDGMENTS

REFERENCES

1. P. Gath, U. Johann, H. R. Schulte, D. Weise, and M. Ayre. LISA system design overview. In *Laser interferometer space antenna- 6th international LISA Symposium*, pages 647–653, AIP conference proceedings, 2006.

2. T. Schuldt, H.-J. Kraus, D. Weise, C. Braxmaier, A. Peters, and U. Johann. A heterodyne interferometer for high resolution translation and tilt measurement as optical readout for the LISA inertial sensor. *Proceedings of the 6th International Conference on Space Optics (ICSO 2006)*, 2006.

3. T. Schuldt, M. Gohlke, D. Weise, U. Johann, A. Peters, and C. Braxmaier. Compact laser interferometer for translation and tilt measurement as optical readout for the LISA inertial sensor. *Proceedings of SPIE*, 6717:Optomechatronic Sensors and Instrumentation III, 67160F, 2007.

4. T. Schuldt, M. Gohlke, D. Weise, U. Johann, A. Peters, and C. Braxmaier. Compact laser interferometer for translation and tilt metrologie. *International Journal of Optomechatronics*, 1, 2007.

5. C.M. Wu, S.T. Lin, and J. Fu. Heterodyne interferometer with two spatial-separated polarization beams for nanometrology. *Opt. Quantum Electron.*, 34(12):1267–1276, 2002.

6. E. Morrison, B. J. Meers, D. I. Robertson, and H. Ward. Automatic alignment of optical interferometers. *Appl. Opt.*, 33(22):5041–5049, 1994.

7. E. Morrison, B. J. Meers, D. I. Robertson, and H. Ward. Experimental demonstration of an automatic alignment system for optical interferometers. *Appl. Opt.*, 33(22):5037–5040, 1994.

8. J. Cordero, T. Heinrich, T. Schuldt, M. Gohlke, S. Lucarelli, D. Weise, U. Johann, A. Peters, and C. Braxmaier. Picometer resolution interferometric characterization of the dimensional stability of zero CTE CFRP. *Proceeding of SPIE*, 7018:Advanced optical and mechanical technologies in telescopes and instrumentation, 2008.